Harmonic Functions for Three-Dimensional Shape Estimation in Cylindrical Coordinates

Tim Baur[1], Johannes Reuter[1], Antonio Zea[2], and Uwe D. Hanebeck[2]

***Abstract*— With the high resolution of modern sensors such as multilayer LiDARs, estimating the 3D shape in an extended object tracking procedure is possible. In recent years, 3D shapes have been estimated in spherical coordinates using Gaussian processes, spherical double Fourier series or spherical harmonics. However, observations have shown that in many scenarios only a few measurements are obtained from top or bottom surfaces, leading to error-prone estimates in spherical coordinates. Therefore, in this paper we propose to estimate the shape in cylindrical coordinates instead, applying harmonic functions. Specifically, we derive an expansion for 3D shapes in cylindrical coordinates by solving a boundary value problem for the Laplace equation. This shape representation is then integrated in a plain greedy association model and compared to shape estimation procedures in spherical coordinates. Since the shape representation is only integrated in a basic estimator, the results are preliminary and a detailed discussion for future work is presented at the end of the paper.**

I. Introduction

In recent years, point cloud sensors such as LiDARs and RADARs have evolved rapidly in such a way that the resolution and accuracy have steadily increased. With nowadays devices, the extent of a target is typically larger than a single sensor cell leading to a vast amount of measurements per time step. Thus, the assumption of point targets is not valid anymore, and objects to be tracked have to be modeled as extended targets leading to the realm of extended object tracking (EOT). An overview of EOT methods can be found in [1], [2].

At the beginning of EOT, numerous papers were published processing 2D data in various applications using different sensor devices. Explicit shapes can be used if prior knowledge is available or computation time is to be kept low. Elliptical shapes [3], [4], [5], [6], [7] can be applied in various applications for different sensors such as LiDAR or RADAR. An overview of elliptic EOT can be found in [8]. Furthermore, rectangular shapes [9], [10], [11], [12] are fundamental in automotive applications as they are very similar to the shape of a car. If no prior knowledge of the target is available and detailed shape information is desired, the shape itself can be estimated during the tracking procedure using Fourier series [13] or Gaussian processes [14]. Finally, learned spatial distribution models [15], [16], [17] can be applied if measurements of a specific sensor and targets to be tracked are available so the model can be adapted to these measurements.

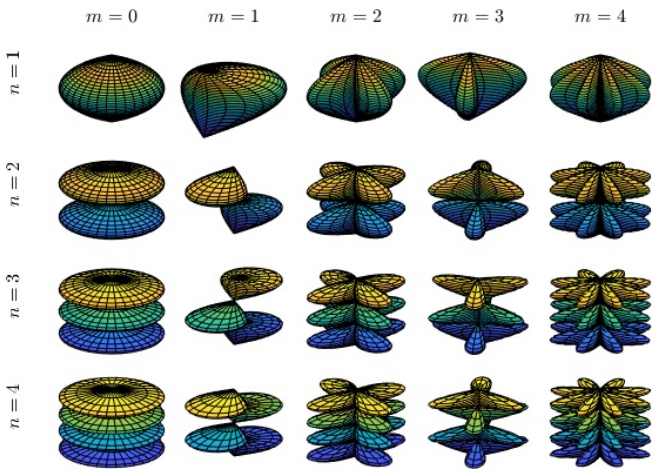

Fig. 1. Basis functions for shape estimation in cylindrical coordinates.

Since modern devices such as multilayer LiDAR sensors or depth cameras produce high-quality 3D point clouds, performing EOT in 3D space is also recommended in many applications. Thus, explicit shapes such as cylinders [18], [19] or ellipsoids [3], [4] can be applied. Besides, many different shapes can be defined using non-uniform rational B-spline (NURBS) surfaces [20], comparable to the B-spline model of [12]. Like in 2D space, estimating the shape itself is finally also possible in 3D space. Here, a 2D radial function can be learned for star-convex shapes. This function can be expanded using Gaussian processes [21], spherical double Fourier series [22], or spherical harmonics [23]. In a filtering procedure, the coefficients of these expansions can then be estimated.

The idea of this paper is based on the observation that in many applications only a few or absolutely no measurements of the target's top or bottom part can be expected. If the shape is estimated using a star-convex spherical radial function, information of these parts is missing, leading to inaccurate estimates. Therefore, the contribution of this paper is to propose a star-convex radial function in cylindrical coordinates describing the surface of the target where a sufficient amount of measurements can be expected. Analogously to spherical harmonics, this radial function can be obtained by solving a boundary value problem (BVP) for Laplace's equation in cylindrical coordinates. The solutions of Laplace's equation are called harmonic functions. In the case of cylindrical coor-

[1]T. Baur and J. Reuter are with the Institute of System Dynamics (ISD), University of Applied Sciences Konstanz (HTWG), Germany, Email: tbaur@htwg-konstanz.de, jreuter@htwg-konstanz.de

[2]A. Zea and U. D. Hanebeck are with the Intelligent Sensor-Actuator-Systems Laboratory (ISAS), Institute for Anthropomatics and Robotics, Karlsruhe Institute of Technology (KIT), Germany, Email: antonio.zea@kit.edu, uwe.hanebeck@kit.edu

dinates and adequate boundary conditions, a double Fourier series expansion for the radial function arises, which can be applied to approximate any continuous star-convex shape. In particular, the solution of the Laplace equation leads to cylindrical basis functions, depicted in Fig. 1, which can be superposed in a series expansion for the approximation procedure. Furthermore, this series expansion is then integrated into a measurement function for 3D extended targets. By adding the Fourier coefficients to the system state, the shape can be estimated by fusing recorded measurements. Since the objective of this paper is to propose the series expansion for cylindrical shape estimation and to present further details on the connection of Laplace's equation, harmonic functions, and shape representations, only a basic measurement model is used to demonstrate the viability of the shape representation. Further improvements in the estimation procedure are left to future work, which is discussed in detail in the last section.

The remainder of this paper is structured as follows. In Sec. II, further information on harmonic functions as solutions to Laplace's equation and the connection to shape representations are given. Then, in Sec. III the BVP for Laplace's equation in cylindrical coordinates and the harmonic series expansion for a star-convex radial shape representation are presented. In Sec. IV, this shape representation is then integrated into a basic measurement model, namely a greedy association model (GAM) for 3D shapes [19], to be able to perform a fusion procedure of noisy point measurements. Afterward, in Sec. V the shape estimation in cylindrical coordinates is compared to shape estimation in spherical coordinates in a static simulated scenario in order to clarify the advantages of the new proposed algorithm. The paper ends with the conclusion and a detailed discussion for future work in Sec. VI.

II. Harmonic functions

Harmonic functions [24, Ch. 1] are special functions solving Laplace's equation given as

$$\nabla^2\varphi = \frac{\partial^2\varphi}{\partial x^2} + \frac{\partial^2\varphi}{\partial y^2} + \frac{\partial^2\varphi}{\partial z^2} = 0 \tag{1}$$

in Cartesian coordinates [25, pp. 49–52]. Here, φ is a scalar function $\varphi : \Phi \to \mathbb{R}$ with $\varphi = \varphi(\underline{x})$ and $\Phi \subset \mathbb{R}^n$. Since we aim to use the solution of a BVP of Laplace's equation for shape representation, we are only interested in non-trivial functions φ. In this section, we want to give some details on why harmonic functions can be used for our shape estimation procedure. In physics, Laplace's equation is used to describe potential fields such as the electrical or gravitational field [26, pp. 68–79]. Besides describing potential laws in physics, harmonic functions have some important properties [24, Ch. 1]:

- *Time invariant*: Harmonic functions are time invariant, meaning that $\frac{\partial\varphi}{\partial t} = 0$ and the function is not changing over time.
- *Translation invariant*: Harmonic functions are translation invariant, meaning that any harmonic function provided with a translation transformation is again a harmonic function.
- *Rotation invariant*: Harmonic functions are rotation invariant, meaning that any harmonic function provided with a rotation transformation is again a harmonic function.
- *Continuity*: Harmonic functions are continuous. Moreover, sums and scalar multiples of harmonic functions are harmonic again due to the linearity of Laplace's equation.
- *Real analytic*: Harmonic functions are real analytic, meaning that any harmonic function is infinitely differentiable and can locally be given as a Taylor series.

All these properties make harmonic functions a good choice for shape representation. Furthermore, as will be seen in the next section, Laplace's equation can be given in any other coordinate system, such as cylindrical coordinates. A BVP can be defined, which describes the given problem, and solutions can be used for the shape estimation procedure. Finally, we want to mention that spherical harmonics can be derived from Laplace's equation in spherical coordinates [26, pp. 786–793] [25, pp. 188–196] and have shown to be applicable to spherical shape estimation [23].

III. Shape representation in cylindrical coordinates

This section presents the BVP for Laplace's equation in cylindrical coordinates and the solution applied for our shape estimation procedure. First of all, for a vector $\underline{x} = [r, \theta, z]^T$ in cylindrical coordinates, Laplace's equation is given as

$$\nabla^2\varphi = \frac{\partial^2\varphi}{\partial r^2} + \frac{1}{r}\frac{\partial\varphi}{\partial r} + \frac{1}{r^2}\frac{\partial^2\varphi}{\partial\theta^2} + \frac{\partial^2\varphi}{\partial z^2} = 0. \tag{2}$$

The BVP is defined through the boundary conditions:

1: $0 < r < R_1,\ 0 < z < h$
2: $\varphi(r,\theta,0) = \varphi(r,\theta,h) = 0$
3: $\varphi(R_1,\theta,z) = f(\theta,z)$
4: $\varphi(r,0,z) = \varphi(r,2\pi,z),\ \frac{\partial\varphi}{\partial\theta}|_{\theta=0} = \frac{\partial\varphi}{\partial\theta}|_{\theta=2\pi}.$

The first boundary condition specifies the variables r and z as being bounded with $R_1 \in \mathbb{R}_{>0}$ and $h \in \mathbb{R}_{>0}$. The second implies that the cylinder is finite, with the function being 0 at the top and bottom. The third one defines the outer contour of the cylinder as only being dependent on the variables θ and z. This condition is crucial, as we actually want our shape-defining radial function to depend only on those two variables. The last condition specifies the function being 2π periodic in the angular variable.

The partial differential equation (2) can be solved using separation of variables by assuming that the function $\varphi(\underline{x})$ can be represented as the product

$$\varphi(\underline{x}) = R(r)\cdot\Theta(\theta)\cdot Z(z). \tag{3}$$

Thus, every function is only dependent on a single cylindrical coordinate. A detailed solution of this BVP can be found in [25, pp. 149–151]. We therefore only present the main

results here in this paper. First of all, the solution of the height variable z is given as

$$Z_n(z) = \sin\left(\frac{n\pi z}{h}\right) \tag{4}$$

with an infinite number of solutions and $n \in \mathbb{N}_0$. Furthermore, the solution of the angular variable θ is given as

$$\Theta_m^{(1)}(\theta) = \sin(m\theta)\,, \Theta_m^{(2)}(\theta) = cos(m\theta) \tag{5}$$

also with an infinite number of solutions and $m \in \mathbb{N}_0$. Finally, the solution of the radial variable r is given as

$$R_{mn}(r) = \frac{I_m(nr)}{I_m(nR_1)} \tag{6}$$

with $I_m(nr)$ being the Bessel functions [26, Ch. 11] of the first kind. In (6), it can be seen that $R_{mn}(r) = 1$ at the boundary if $r = R_1$. Due to the linearity of Laplace's equation, the general solution of the BVP in cylindrical coordinates can be given as

$$\begin{aligned} f(\theta,z) = &\frac{1}{2}\sum_{n=1}^{n_z} a_{n0}\sin\left(\frac{n\pi z}{h}\right) \\ &+ \sum_{n=1}^{n_z}\sum_{m=1}^{n_\theta}\sin\left(\frac{n\pi z}{h}\right)\left(a_{nm}\cos(m\theta) + b_{nm}\sin(m\theta)\right). \end{aligned} \tag{7}$$

with an amount of $2n_\theta n_z + n_z$ coefficients a_{n0}, a_{nm}, $b_{nm} \in \mathbb{R}$. As can be seen from (7), the basis functions on the outer contour of a finite cylinder, depicted in Fig. 1, are given as

$$\Psi_{nm}(\theta,z) = \sin\left(\frac{n\pi z}{h}\right)\left(\cos(m\theta) + \sin(m\theta)\right). \tag{8}$$

If $n_\theta = n_z = \infty$, (7) gives an exact representation of any continuous function on the outer surface of a finite cylinder. However, because of computational reasons, we restrict the sums in (7) to be finite.

If the shape should involve a vertical plane of symmetry in parallel to the local xz-plane of the object, it is possible to modify (7) to be even in the radial variable θ. Similar to [22], this can be achieved by discarding the sine components of θ. This modification results in the radial function

$$\begin{aligned} f(\theta,z) = &\frac{1}{2}\sum_{n=1}^{n_z} a_{n0}\sin\left(\frac{n\pi z}{h}\right) \\ &+ \sum_{n=1}^{n_z}\sum_{m=1}^{n_\theta} a_{nm}\cos(m\theta)\sin\left(\frac{n\pi z}{h}\right) \end{aligned} \tag{9}$$

with an amount of $n_\theta n_z + n_z$ coefficients a_{n0}, $a_{nm} \in \mathbb{R}$. Using either (7) or (9), the radial function for our shape can be expanded and learned during the tracking procedure, as will be seen in the following. Especially, (9) is of particular interest for real-world applications as many targets such as cars involve a vertical plane of symmetry, and only measurements of half the target can be expected for single sensor applications. In these settings, the unseen backside of the target can be modeled using symmetry assumptions. Please note that shape representation using (9) in comparison to (7) even requires less coefficients. Throughout this paper, we will refer to (7) and (9) as cylindrical double Fourier series (CDFS) without and with a vertical plane of symmetry, respectively.

IV. A BASIC ESTIMATOR

In this section, a greedy association model (GAM) [19] for shape estimation using either (7) or (9) is presented. First of all, the system state comprises the position $\underline{m}_k$, the orientation ϕ_k, the height h_k, and the shape vector $\underline{p}_k$ and reads as

$$\underline{x}_k = \left[\underline{m}_k^T, \phi_k^T, h_k^T, \underline{p}_k^T\right]^T. \tag{10}$$

In this paper, the shape vector is given as $\underline{p}_k = [a_{01}, a_{02}, \ldots, a_{11}, a_{12}, \ldots, b_{11}, b_{12}, \ldots]^T$ for a CDFS without vertical plane of symmetry and as $\underline{p}_k = [a_{01}, a_{02}, \ldots, a_{11}, a_{12}, \ldots]^T$ for a CDFS with vertical plane of symmetry. Please note that we restrict ourselves to orientations ϕ in the xy-plane in this paper. However, all three rotation angles can also be integrated into the system state and the following measurement model. Furthermore, we change the height variable z of the cylindrical coordinates as $z = uh$ with $u \in [0,1]$ to involve the estimated height. The solution of the height variable (4) in Laplace's equation then changes to $Z_n(z) = \sin(n\pi u)$ and is only dependent of the parameter u. Please note that the basis functions (8) and both the CDFS (7) with vertical plane of symmetry and the CDFS without (9) are only dependent on the parameter u now, as well.

In order to estimate the hidden system state $\underline{x}_k$, we require a measurement model that relates received measurements to the system state. First of all, we assume to receive a measurement set $\mathscr{Y}_k = \left\{\underline{y}_{k,l}\right\}_{l=1}^{n_k}$ with a varying amount of measurements n_k every time step k. We further assume these measurements to be mutually independent. Thus, it is sufficient only to give the measurement equation for a single measurement. In the filter, this measurement equation can then be applied to all received measurements [18]. In this paper, measurements are assumed to be gathered based on a measurement source model

$$\underline{y}_{k,l} = \underline{z}_{k,l} + \underline{v}_{k,l} \tag{11}$$

with measurement source $\underline{z}_{k,l}$ and white Gaussian zero-mean noise term $\underline{v}_{k,l} = \mathscr{N}(\underline{0}, \mathbf{C}_{\underline{v}})$. The measurement equation can then directly be given as

$$\underline{y}_{k,l} = \underline{m}_k + \mathbf{R}_{\phi_k} \cdot \begin{bmatrix} f(\theta_{k,l}, u_{k,l}) \cdot \cos(\theta_{k,l}) \\ f(\theta_{k,l}, u_{k,l}) \cdot \sin(\theta_{k,l}) \\ u_{k,l} \cdot h_k \end{bmatrix} + \underline{v}_{k,l} \tag{12}$$

in Cartesian coordinates with the rotation matrix $\mathbf{R}_{\phi_k}$ in the xy-plane and the CDFS (7) or (9). Since we do not know the exact measurement source, we are faced with the measurement source association problem for 3D shape estimation [19]. In our case of 3D EOT, the measurement source is defined through the parameters u and θ. Therefore, the likelihood for this estimation problem can be given as the marginal distribution

$$p\left(\underline{y}|\underline{x}\right) = \int_{u=0}^{1}\int_{\theta=0}^{2\pi} p\left(\underline{y}|\underline{x},\theta,u\right)\cdot p\left(\theta,u|\underline{x}\right) d\theta\, du \tag{13}$$

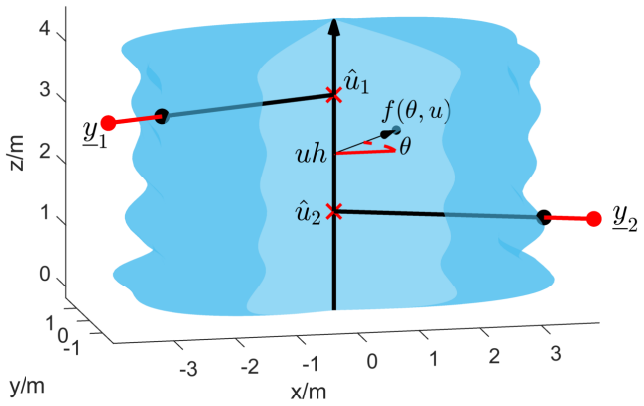

Fig. 2. Illustration of the radial function $f(\theta,u)$ and the measurement source association. Measurements are red balls, measurement sources are black balls.

with the first part $p\left(\underline{y}|\underline{x},\theta,u\right)$ being the sensor model and the second part $p\left(\theta,u|\underline{x}\right)$ being the source model. More details on modeling 3D extended targets can be found in [27, Ch. 3]. Please note that we omitted indices k,l in the likelihood description since it is equal for every measurement in every time step. In [18], [19] several solutions to 3D EOT are presented. In our study, we restrict ourselves to the most basic model, a GAM. For this model, the mass of the source model is reduced to a single point and can be given as the Dirac δ-distribution $p(\theta,u|\underline{x}) = \delta(\theta-\hat{\theta},u-\hat{u})$ with $\hat{\theta}$ and $\hat{u}$ being the parameters of the most likely measurement source. The likelihood (13) then reduces to the Gaussian distribution

$$p\left(\underline{y}|\underline{x}\right) = \mathcal{N}\left(\underline{y};\hat{\underline{z}},\mathbf{C}_{\underline{v}}\right) \tag{14}$$

with the most likely measurement source $\hat{\underline{z}}$.

We use two basic assignment assumptions for the most likely measurement source to show the distinct advantages of shape estimation in cylindrical compared to spherical coordinates in specific scenarios. The first step is to calculate the measurement in local coordinates as

$$\tilde{\underline{y}}_{k,l} = \mathbf{R}_{\phi_k}^{-1} \cdot (\underline{y}_{k,l} - \underline{m}_k). \tag{15}$$

The angular parameter of the cylindrical contour is then assumed to be given through the angle

$$\hat{\theta}_{k,l} = \operatorname{atan2}(\tilde{\underline{y}}^y_{k,l}, \tilde{\underline{y}}^x_{k,l}) \tag{16}$$

with $\tilde{\underline{y}}^x_{k,l}$ and $\tilde{\underline{y}}^y_{k,l}$ being the x and y components of the measurement $\tilde{\underline{y}}_{k,l}$ in local coordinates, respectively. Furthermore, the height parameter is calculated as

$$\hat{u}_{k,l} = \begin{cases} 0 & \tilde{\underline{y}}^z_{k,l} < 0 \\ \frac{\tilde{\underline{y}}^z_{k,l}}{h} & 0 \leq \tilde{\underline{y}}^z_{k,l} \leq h \\ 1 & \tilde{\underline{y}}^z_{k,l} > h \end{cases} \tag{17}$$

with $\tilde{\underline{y}}^z_{k,l}$ being the z component of the measurement $\tilde{\underline{y}}_{k,l}$ in local coordinates. An illustration of the radial function and the measurement source association scheme is depicted in Fig. 2. With these assumptions, we can define our measurement source and include the measurement equation (12) into a nonlinear state estimation procedure. This paper uses a smart sampling Kalman filter (S²KF) [28], [29] for state estimation. Please note that the approach for the measurement source association problem proposed in this paper is a fundamental solution. Investigations [27, pp. 74–79] showed that height estimation could be biased using a GAM. However, as will be seen in the next section, this measurement model is already superior to shape estimation in spherical coordinates and is therefore used to present the advantages of our shape estimation method. Further details on improvements and future work will be given in the last section VI.

V. Comparison to Shape Estimation in Spherical Coordinates

This section compares our shape estimation procedure to shape estimation in spherical coordinates. Specifically, we compare it to spherical radial shape representations using spherical harmonics (SH) [23], spherical double Fourier series (SDFS) [22], and Gaussian processes (GP) [21]. Like our procedure for cylindrical shape estimation, we implemented all comparison algorithms using an S²KF [28], [29]. Here, the system state is sampled with 10 samples per dimension for each shape estimation procedure. This paper investigates the shape estimation performance in a simulated static scenario. Therefore, measurements from a cuboid with a length of 6 m, a width of 3 m, and a height of 4 m are generated uniformly distributed from half the hull and no measurements from the top or bottom surfaces of the cuboid. We compare the performance of each algorithm with the well-known intersection-over-union (IOU) measure given by

$$\mathrm{IOU}(S_t,S_e) = \frac{\mathrm{volume}(S_t \cap S_e)}{\mathrm{volume}(S_t \cup S_e)} \tag{18}$$

with the true shape S_t and the estimated shape S_e. Please note that this measure evaluates the performance of the shape estimate as well as the position and rotation estimate and is, therefore, a good overall measure to compare shape estimation procedures.

In our simulation, we generated 2000 measurements and performed an update for every filter and every single measurement. Measurements are corrupted by isotropic measurement noise with a standard deviation of $\sigma_{\underline{v}} = 0.2\,\mathrm{m}$. We choose a relatively high standard deviation for the measurement noise to emphasize the estimation performance. Since the measurements are drawn from half the hull of the cuboid, we applied the radial function (9) with a vertical plane of symmetry for cylindrical shape estimation. Also, for shape estimation in spherical coordinates, a vertical plane of symmetry is applied for every algorithm to model the unseen backside. For a better overall comparison, we used an equal amount of coefficients for every model where the shape is expanded with a truncated sum, namely CDFS, SH, and SDFS. For cylindrical shape estimation we choose $n_\theta = 8$ and $n_u = 9$ resulting in 81 coefficients. For spherical shape estimation using SH, we used 81 coefficients as well and 73 coefficients for SDFS. For the model where the shape is learned using a GP, we choose to use 210 basis points.

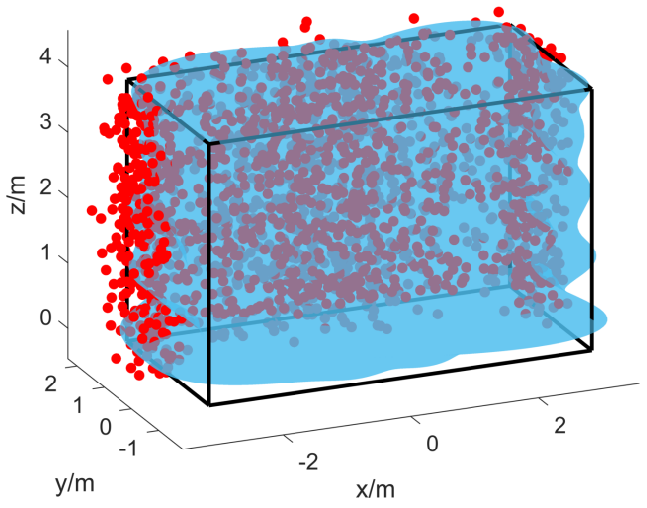

Fig. 3. Estimated shape (blue surface) at the end of a scenario with generated measurements (red balls). The reference cuboid is shown with black lines.

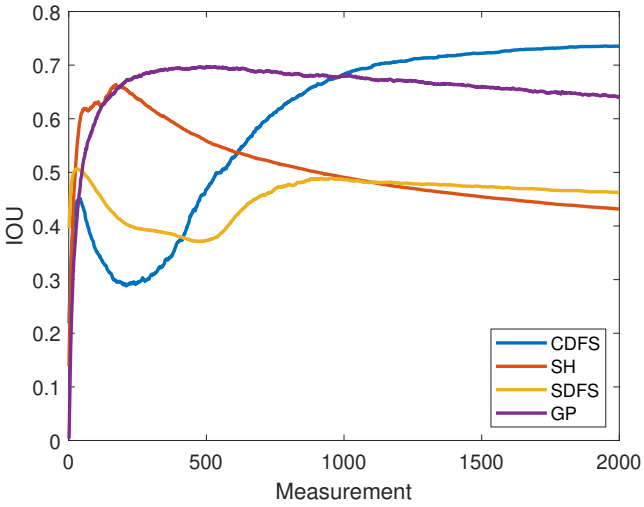

Fig. 4. IOU measures for every shape estimation procedure.

Every filter position and orientation was initialized with the reference as this study was intended to investigate the overall shape estimation quality. Variances for the position and orientation were initialized with 1. The shape coefficients were initialized to be a ball of radius 2 for SH and SDFS, and $\underline{p} = [3, 0, \ldots, 0]^T$ for the coefficients of cylindrical shape estimation. Variances were initialized as 5 for every shape coefficient. The initialization procedure presented in [21] was used for GP.

In Fig. 3, the result of cylindrical shape estimation at the end of a scenario is depicted. Furthermore, the simulation environment with the reference cuboid and measurements from one half of the cuboid hull are depicted. The shape is approximated well at the end of the scenario. As seen, the height is slightly overestimated, which emanates from the GAM as this model is known to produce biased height estimates. Moreover, the Gibbs phenomenon [26, pp. 910–914] is a problem we face in the series for the height parameter u. The oscillation of the illustrated shape is more significant at the top and bottom, what can be tied to the Gibbs phenomenon as we have discontinuities in these parts of the shape.

In Fig. 4, IOU measures of a Monte Carlo simulation with 100 runs are depicted. As seen, even with the basic estimator we used in this paper, we get the best performance using cylindrical shape estimation in this scenario. Moreover, every shape estimation procedure applying spherical coordinates diverges in this simulation. Since information from the top and bottom part of the target is missing, where spherical radial functions are defined as well, this estimate is error-prone. Shape estimation applying cylindrical coordinates, however, converges. Furthermore, the CDFS IOU gets worse at the beginning of the scenario. This can be explained with few information at the beginning of the scenario leading to larger outbursts in the shape. However, with more measurements and more information, the estimate gets better and converges at the end of the scenario. Finally, we also measured the estimation time for a single update for every filter. The simulation was performed using MATLAB R2022a on an Intel(R) Xeon(R) X5680 CPU with 3.33 GHz. It turned out that computation time for filters using expansions for the radial function was nearly the same with roughly 5 ms. Merely computation time for GP was much slower with about 85 ms. Overall, shape estimation in cylindrical coordinates showed clear advantages compared to shape estimation in spherical coordinates.

VI. Conclusion and Future Work

This paper proposes a new method for 3D shape estimation in cylindrical coordinates using harmonic functions. The derivation of the radial function is based on the solution of a BVP of Laplace's equation in cylindrical coordinates. The general solution of this problem on the outer surface of a finite cylinder can be given as a CDFS. We proposed a basic measurement model to solve the measurement source association problem using a GAM. Static simulations with measurements from half the hull of a cuboid and comparisons to shape estimation in spherical coordinates showed the superiority of cylindrical over spherical radial functions if no measurements of the top and bottom part of the target are available. Moreover, the results are particularly impressive since GAMs are known to be biased for height estimation. In the static simulation, we showed that shape estimation diverges for every model applying spherical radial functions in contrast to cylindrical ones that converge.

Since we are just using a basic GAM in this paper, we want to give detailed thoughts for future work. In [27, pp. 74–79], it was shown that a robust height estimate can only be achieved if the likelihood is reformulated to combine two different association approaches in a single model. When reformulating a random hypersurface model (RHM) [4], [13] for 3D EOT to an extrusion RHM [18], [19], [30], a GAM is applied for the angular and a spatial distribution model for the height association. This combination proved to be

the most suitable compared to a GAM. Future work will therefore concentrate on implementing an extrusion RHM for cylindrical shape estimation. These models can either be integrated into an S²KF [19] or in nonlinear estimators like the progressive Gaussian filter [31], [32]. When using an S²KF, only unimodal Gaussian distributions can be utilized for the height distribution. However, in general, the height distribution will be multimodal for real-world shapes leading to the necessity of applying Gaussian mixture distributions or nonlinear estimators. Calculations have already shown that the height distribution can be derived from the CDFS. Central will therefore be to integrate this height distribution into a suitable estimation procedure.

Further improvement is needed to get a deeper understanding of the Gibbs phenomenon [26, pp. 910–914] in cylindrical shape estimation. Real-world targets often comprise discontinuities in their shapes where the Gibbs phenomenon causes larger outbursts. Future work will, therefore, also focus on understanding the Gibbs phenomenon for these targets and on studies to reduce it.

Finally, we will apply our shape estimation procedure to real-world measurements from moving and rotating targets recorded with different sensors in varying scenarios. These investigations are also necessary since the assumption of no measurements at the top and bottom part will not pertain for every scenario. Rather, it will be the case that some measurements can occur in these areas of the target. Handling these measurements will therefore also be part of future work.

References

[1] K. Granström, M. Baum, and S. Reuter, "Extended object tracking: Introduction, overview, and applications," *Journal of Advances in Information Fusion*, vol. 12, Dec. 2017.

[2] L. Mihaylova, A. Y. Carmi, F. Septier, A. Gning, S. K. Pang, and S. Godsill, "Overview of Bayesian sequential Monte Carlo methods for group and extended object tracking," *Digital Signal Processing*, vol. 25, pp. 1–16, 2014.

[3] M. Feldmann, D. Fränken, and W. Koch, "Tracking of extended objects and group targets using random matrices," *IEEE Transactions on Signal Processing*, vol. 59, no. 4, pp. 1409–1420, 2011.

[4] M. Baum, B. Noack, and U. D. Hanebeck, "Extended object and group tracking with elliptic random hypersurface models," in *13th International Conference on Information Fusion (FUSION)*, 2010, pp. 1–8.

[5] F. Govaers, "On independent axes estimation for extended target tracking," in *2019 Sensor Data Fusion: Trends, Solutions, Applications (SDF)*, 2019, pp. 1–6.

[6] K. Thormann and M. Baum, "Fusion of elliptical extended object estimates parameterized with orientation and axes lengths," *IEEE Transactions on Aerospace and Electronic Systems*, vol. 57, no. 4, pp. 2369–2382, 2021.

[7] P. Hoher, S. Wirtensohn, T. Baur, J. Reuter, F. Govaers, and W. Koch, "Extended target tracking with a lidar sensor using random matrices and a virtual measurement model," *IEEE Transactions on Signal Processing*, vol. 70, pp. 228–239, 2022.

[8] K. Thormann, S. Yang, and M. Baum, "A comparison of Kalman filter-based approaches for elliptic extended object tracking," in *IEEE 23rd International Conference on Information Fusion (FUSION)*, 2020, pp. 1–8.

[9] K. Granström, C. Lundquist, and U. Orguner, "Tracking rectangular and elliptical extended targets using laser measurements," in *14th International Conference on Information Fusion (FUSION)*, 2011.

[10] C. Knill, A. Scheel, and K. Dietmayer, "A direct scattering model for tracking vehicles with high-resolution radars," in *IEEE Intelligent Vehicles Symposium (IV)*, 2016, pp. 298–303.

[11] P. Broßeit, M. Rapp, N. Appenrodt, and J. Dickmann, "Probabilistic rectangular-shape estimation for extended object tracking," in *IEEE Intelligent Vehicles Symposium (IV)*, 2016, pp. 279–285.

[12] H. Kaulbersch, J. Honer, and M. Baum, "A Cartesian B-spline vehicle model for extended object tracking," in *21st International Conference on Information Fusion (FUSION)*, 2018.

[13] M. Baum and U. D. Hanebeck, "Shape tracking of extended objects and group targets with star-convex RHMs," in *14th International Conference on Information Fusion (FUSION)*, 2011.

[14] N. Wahlström and E. Özkan, "Extended target tracking using Gaussian processes," *IEEE Transactions on Signal Processing*, vol. 63, no. 16, pp. 4165–4178, 2015.

[15] A. Scheel and K. Dietmayer, "Tracking multiple vehicles using a variational radar model," *IEEE Transactions on Intelligent Transportation Systems*, vol. 20, no. 10, pp. 3721–3736, 2019.

[16] H. Kaulbersch, J. Honer, and M. Baum, "EM-based extended target tracking with automotive radar using learned spatial distribution models," in *2019 22th International Conference on Information Fusion (FUSION)*, 2019, pp. 1–8.

[17] J. Honer and H. Kaulbersch, "Bayesian extended target tracking with automotive radar using learned spatial distribution models," in *2020 IEEE International Conference on Multisensor Fusion and Integration for Intelligent Systems (MFI)*, 2020, pp. 316–322.

[18] F. Faion, M. Baum, and U. D. Hanebeck, "Tracking 3D shapes in noisy point clouds with random hypersurface models," in *15th International Conference on Information Fusion (FUSION)*, 2012, pp. 2230–2235.

[19] F. Faion, A. Zea, J. Steinbring, M. Baum, and U. D. Hanebeck, "Recursive Bayesian pose and shape estimation of 3D objects using transformed plane curves," in *Sensor Data Fusion: Trends, Solutions, Applications (SDF)*, 2015.

[20] B. Naujoks, P. Burger, and H.-J. Wuensche, "Fast 3D extended target tracking using NURBS surfaces," in *2019 IEEE Intelligent Transportation Systems Conference (ITSC)*, 2019, pp. 1104–1109.

[21] M. Kumru and E. Özkan, "Three-dimensional extended object tracking and shape learning using Gaussian processes," *IEEE Transactions on Aerospace and Electronic Systems*, vol. 57, no. 5, pp. 2795–2814, 2021.

[22] T. Baur, J. Reuter, A. Zea, and U. D. Hanebeck, "Shape estimation and tracking using spherical double Fourier series for three-dimensional range sensors," in *2021 IEEE International Conference on Multisensor Fusion and Integration for Intelligent Systems (MFI)*, 2021, pp. 1–6.

[23] G. Kurz, F. Faion, F. Pfaff, A. Zea, and U. D. Hanebeck, "Three-dimensional simultaneous shape and pose estimation for extended objects using spherical harmonics," 2020.

[24] S. Axler, S. Ramey, P. Bourdon, R. Wade, and S. S. Media, *Harmonic Function Theory*, ser. Graduate Texts in Mathematics. Springer, 2001.

[25] H. Weinberger, *A First Course in Partial Differential Equations with Complex Variables and Transform Methods*. Wiley, 1965.

[26] G. B. Arfken, H.-J. Weber, and F. E. Harris, *Mathematical Methods for Physicists*. Oxford: Academic, 2012.

[27] F. Faion, "Tracking extended objects in noisy point clouds with application in telepresence systems," Ph.D. dissertation, Karlsruher Institut für Technologie (KIT), 2016.

[28] J. Steinbring and U. D. Hanebeck, "S2KF: The smart sampling Kalman filter," in *Proceedings of the 16th International Conference on Information Fusion (FUSION)*, 2013, pp. 2089–2096.

[29] J. Steinbring, "Nonlinear estimation toolbox." [Online]. Available: https://bitbucket.org/nonlinearestimation/toolbox

[30] A. Zea, F. Faion, and U. D. Hanebeck, "Tracking extended objects using extrusion random hypersurface models," in *Sensor Data Fusion: Trends, Solutions, Applications (SDF)*, 2014.

[31] J. Steinbring and U. D. Hanebeck, "Progressive Gaussian filtering using explicit likelihoods," in *17th International Conference on Information Fusion (FUSION)*, 2014, pp. 1–8.

[32] J. Steinbring, M. Baum, A. Zea, F. Faion, and U. D. Hanebeck, "A closed-form likelihood for particle filters to track extended objects with star-convex RHMs," in *2015 IEEE International Conference on Multisensor Fusion and Integration for Intelligent Systems (MFI)*, 2015, pp. 25–30.